Renewable Energy 222 (2024) 119833

Contents lists available at ScienceDirect

Renewable Energy

journal homepage: www.elsevier.com/locate/renene

Construction of Cu–Ru bimetallic catalyst for the selective catalytic transfer hydrogenation of carbonyl (C═O) in biomass-derived compounds

Bo Cai [a,b,c], Rui Kang [b], Junfeng Feng [b], Thomas L. Eberhardt [d], Zhongqing Ma [a], Qingge Zhu [a], Hui Pan [b,*]

[a] National Engineering Research Center for Wood-based Resource Comprehensive Utilization, College of Chemistry and Materials Engineering, Zhejiang A & F University, Hangzhou, 311300, China
[b] International Innovation Center for Forest Chemicals and Materials, Nanjing Forestry University, Nanjing, 210037, China
[c] International Joint Research Center for Biomass Materials, Southwest Forestry University, Kunming, 650224, China
[d] Forest Products Laboratory, USDA Forest Service, One Gifford Pinchot Drive, Madison, WI, 53726, USA

ARTICLE INFO

Keywords:
Biomass conversion
Catalytic transfer hydrogenation
Bimetallic catalyst
Carbonyl compounds
Effects of heteroatom

ABSTRACT

The catalytic transfer hydrogenation (CTH) of levulinate ester to γ-valerolactone is one of the important reactions for production of renewable fuels from biomass. An efficient and robust bimetallic Cu–Ru catalyst were developed for the hydrogenation of biomass-derived ethyl levulinate to γ-valerolactone. A series of bimetallic catalysts were prepared and characterized in detail. Subsequently, the as-prepared catalysts were evaluated in the hydrogenation system of ethyl levulinate. The results showed that Cu–Ru/ZrO_2–SO_3–SiO_2-450 catalyst provided 100 % GVL yield in 12 h at 180 °C. Meanwhile, it also exhibited high catalytic hydrogenation activity for the various biomass-derived carbonyl compounds. The structure-reactivity relationship of catalysts was investigated in detail, and the results show the interaction between support and metal sites played an important role in the hydrogenation activity. The sulfur species could tune the electronic states of metallic sites to gain optimal activity. Besides, the Cu–Ru/ZrO_2–SO_3–SiO_2-450 catalyst performed excellent recyclability in five reaction runs without an obvious loss of activity.

1. Introduction

The exploration and utilization of renewable energy resources to produce sustainable chemicals and biofuels have drawn increasing attention owing to the ever depletion of fossil resources and environmental issues [1,2]. Biomass is one of the sustainable organic carbon resource and represents the largest potential volume for biofuels and biochemical production, including polyols [3], acids [4], esters [5], and aldehydes [6]. For instance, ethyl levulinate, a carbonyl compound derived from lignocellulose biomass, can be converted to γ-valerolactone (GVL) via hydrogenation reaction. GVL has a versatile application in many areas including liquid fuel, food additive, or solvent for organic synthesis [7,8]. Especially, GVL could be blended with gasoline diesel fuel owing to its high heating value and energy density [9].

Heterogeneous catalysts perform a crucial role in the hydrogenation process of biomass-derived compounds into valuable chemicals, which is due to easy separation and recyclable. The metal loaded heterogeneous catalysts, including Pd [10], Pt [11], Ru [12], Cu, Co, and Ni [13], were often used for the hydrogenation of biomass-derived compounds into valuable chemicals in the presence of hydrogen, because of the high catalytic activity, low-cost, stability and recyclability. When H_2 was applied as the H donor, required high pressure in the reaction system brings some issues such as high cost and inconvenient operation conditions. The catalytic transfer hydrogenation (CTH) reaction could use the alcohol as the *in-situ* H-donor for the hydrogenation of the unsaturated bonds, which could replace the high pressures H_2 [14]. For example, Huang et al. reported a trifunctional Hf-bagasse coordination complex-derived catalyst that could provide 99.1 % GVL yield with isopropanol as the solvent and H-donor under a mild reaction condition [15]. Han et al. prepared a support-free mesoporous Ni catalyst for the conversion of ethyl levulinate (EL) to GVL via CTH reaction, and the EL conversion of 100 % and GVL selectivity of 99.1 % were obtained at 180 °C [9]. Tabanelli investigated the conversion of methyl and ethyl levulinates to GVL via CTH reaction under both bath and gas-flow conditions, and their results suggested the hydrogenation of EL could provide the highest GVL yield when 2-propanol was used as the H-donor

* Corresponding author.
E-mail address: hpan@njfu.edu.cn (H. Pan).

https://doi.org/10.1016/j.renene.2023.119833
Received 7 July 2023; Received in revised form 1 November 2023; Accepted 15 December 2023
Available online 28 December 2023

solvent [16].

The catalyst support plays an important role in the catalytic activity of hydrogenation catalyst during CTH reaction process. The catalyst support could affect the catalytic activity of metal sites via the electron effect, steric effect, and microenvironments effect [17,18]. Our group has also reported the CTH of levulinic acid to GVL over the Ru/g-C_3N_4 catalyst. The results indicated that the N sites of the g-C_3N_4 support could tune the electron state of the active metal sites (Ru^0), thus endowing the excellent catalytic activity of this catalyst in the CTH reaction [19]. Besides, Lu et al. suggested that the synergistic effect in a bimetallic oxide usually affects the behavior of supported-metal catalyst. Specifically, the unique synergy in the $Sn_xMn_1O_y$ oxide can boost the hydrogenation catalysis of supported Pt nanoparticles for the selective conversion of LA to GVL [20]. Therefore, it can be seen that the support could enhance the catalytic hydrogenation activity and stability of catalyst.

The reaction condition is an important evaluation criterion in the application process. Previous study demonstrated that the monometallic catalysts presented the excellent catalytic performance in the CTH reactions for the upgradation of biomass platform compounds [21]. However, the low stability and easily oxidized nature of the catalysts severely limited their application in CTH reactions. Hence, the bimetallic catalyst strategy had been developed, which not only improve the stability of catalyst but also enhance the catalytic activity of catalysts [22,23]. The Al_2O_3-based Ni–Cu bimetallic catalysts were studied for the hydrogenation of levulinic acid, which achieved the high yield of γ-valerolactone (96 %) at the reaction condition of 250 °C and 6.5 MPa hydrogen [24]. Besides, Li et al. reported that activated carbon supported bimetallic Ni and Fe catalysts for the hydrogenation of biomass-derived ethyl levulinate into the γ-valerolactone, which could achieve 99.3 % conversion of EL and 99.0 % yield of GVL at the mild reaction condition (100 °C, 4 MPa H_2, 6 h) [25]. However, the harsh reaction (high reaction temperature and hydrogen pressure) and low reaction efficiency in the hydrogenation process of EL limited the production of GVL, as shown in Table 1. Therefore, it is highly desirable to develop economically feasible catalysts for the hydrogenation of EL into GVL.

In this study, the bimetallic Cu–Ru catalyst was prepared for the conversion of biomass-derived platform compounds into the valuable chemicals. The influences of reaction conditions (e.g., temperature, time, catalyst dosage, and medium) on the CTH reaction of EL to GVL over the as prepared catalysts were investigated. Subsequently, the relationship of the structure and activity was investigated by various characterization techniques of X-ray power diffraction (XRD), transmission electron microscopy (TEM/HRTEM), X-ray photoelectron spectroscopy (XPS), H_2 temperature-programmed reduction (H_2-TPR) and the temperature-programmed desorption of ammonia (NH_3-TPD). Besides, the recyclability and stability of the bimetallic Cu–Ru catalyst were evaluated. Finally, the Cu–Ru bimetallic catalyst also was performed in the hydrogenation of other biomass derived compounds into value-added chemicals. The results could provide a new insight for the design of the catalyst in selective hydrogenation process via the regulating the interaction between carriers and active metals.

Table 1
The lists of conversion of EL into GVL over different catalyst.

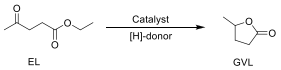

Entry	Catalyst	H-donor	T [°C]	t [h]	GVL yield [%]	Ref.
1	3Pd–10Nb-500-AC	H_2	100	5	81	[26]
2	20%Co/SBA-15	H_2	220	–	96.4	[27]
3	DUT-52(Hf)	2-PrOH	160	5	86	[28]
4	$ZrO(OH)_2{\cdot}xH_2O$	2-PrOH	200	1	88.5	[29]
5	Pt/TiO_2	2-PrOH	110	24	91	[30]
6	Ru/UiO-66	H_2	80	1	50	[31]
7	MoS_2/AC	H_2	230	1.5	88.7	[32]

2. Experimental

2.1. Materials

ZrO_2–SO_3–SiO_2, ZrO_2, and SiO_2 supports were purchased from Saint-Gobain NorPro Company (USA). $Cu(NO_3)_2{\cdot}6H_2O$ and all the alcohol solvents (i.e., methanol, ethanol, 2-propanol (2-PrOH), 2-butanol (2-BuOH), and 3-pentanol) were purchased from Sinopharm Chemical Reagent Company (Shanghai, China). $RuCl_3$ (Ru, 37 %) was purchased from Aladdin Chemical Company (Shanghai, China). Levulinic acid, levulinate esters, and γ-valerolactone were purchased from Energy Chemical Reagent Company (Shanghai, China). Furfural, benzaldehyde, phenylacetaldehyde, and acetophenone were purchased from TCI Chemical Reagent Company (Shanghai, China). All chemicals were of reagent grade and used without further purification.

2.2. Preparation of the catalysts

The catalysts were synthesized by the impregnation method as follows: 1.90 g ZrO_2–SO_3–SiO_2 was dispersed into 50 mL deionized water. Subsequently, 0.3780 g $Cu(NO_3)_2{\cdot}3H_2O$ and 0.2054 g $RuCl_3$ were added to the above suspension. The mixture was stirred for 12 h and then dried at 100 °C overnight. The dried powder was ground and annealed in the muffle furnace at 400 °C for 4 h. Then, the obtained catalyst precursor was reduced under a flow of 5%H_2/N_2 at 450 °C for 2 h with a staged heating method. The detailed steps are as follows: the temperature was heated to 350 °C within 90 min, then raised to 450 °C within 60 min, and kept at 450 °C for 2 h. After cooling down to room temperature, the catalyst was collected. The catalysts also were reduced at three different temperatures (350, 450, and 550 °C) and the catalysts were named as Cu–Ru/ZrO_2–SO_3–SiO_2-350, Cu–Ru/ZrO_2–SO_3–SiO_2-450, Cu–Ru/ZrO_2–SO_3–SiO_2-550, corresponding to the reduction temperatures. For the purpose of comparison, catalysts Cu–Ru/ZrO_2 and Cu–Ru/SiO_2 were also prepared using a similar method as that of Cu–Ru/ZrO_2–SO_3–SiO_2-450 catalyst.

2.3. Hydrogenation reactions with the prepared catalysts

Hydrogenation of EL to GVL was conducted in a thick-wall pressured tube. For a model hydrogenation reaction: EL 1.0 mmol, Cu–Ru/ZrO_2–SO_3–SiO_2-450 100 mg and 2-propanol 5 mL were charged into the reaction tube and mixed well with a magnetic stirrer. The tube was purged with the N_2 to remove air. Then, the reaction tube was allowed to react at 180 °C for 12 h. Upon the end of the reaction, the tube was cooled down to room temperature, and the solution was separated by centrifugation and subjected to analysis. For the recycling experiment of the catalyst, the catalyst was recovered by centrifugation after hydrogenation reaction and washed with 2-PrOH for three times. The recovered catalyst was directly applied for the next run. The products were analyzed by chromatography-mass spectroscopy (GC-MS, Agilent 7890 A, Agilent 5975CMSD) and gas chromatography (GC, Agilent 7890 A) with a DB-5 capillary column (30 m × 0.25 mm × 0.25 mm, Agilent). The temperature of the column increased from160 to 250 °C at a 15 °C/min rate. Naphthalene was used as the internal standard.

2.4. Characterizations of the catalysts

The XRD analysis of the catalysts were performed on an X-ray diffractometer (Rigaku D MAX III VC, Rigaku, Japan). TEM and HRTEM images were acquired on a transmission electron microscopy (JEOL-2010, Japan). The Brunauer-Emmett-Teller (BET) surface area and

porosity of the catalysts were analyzed by N_2 sorption (Tristar II 3020 M, Micromeritics). X-ray photoelectron spectra (XPS) were recorded on the Scientific Escalab 250-X-ray photoelectron spectrometry instrument (SHIMADZU, Japan) using Al Kα X-ray as the excitation source (hν = 1486.6 eV). The NH_3-TPD and H_2-TPR were recorded on a multifunctional atomic adsorption instrument (xianquan, TP-5080, China) equipped with TCD.

3. Results and discussion

3.1. Characterization of as-synthesized catalysts

The XRD patterns of the catalysts were shown in Fig. 1 and S1. Five characteristic peaks at 28.08°, 30.28°, 35.18°, 50.38°, 59.96° presented in the XRD spectrum of pristine ZrO_2–SO_3–SiO_2 support (Fig. 1), corresponding to the ZrO_2 (JCPDS#17-0923) and SiO_2 (JCPDS#47-1144), thus confirming the bimetallic oxides in the support. Notably, two new peaks appeared at the 2θ of 24.04°、40.84° in the calcined ZrO_2–SO_3–SiO_2 pattern (Fig. 1a), which should be attributed to the Si–Zr species (JCPDS#10-0267). This result manifested that the interaction between Si and Zr atoms could be enhanced after the calcination process. Besides, the intensity of the characteristic diffraction peaks of SiO_2 at 28.08° and 55.42° increased compared to that of the pristine support, indicated the increase of SiO_2 crystallinity at the high temperature. Notably, there is no obvious diffraction peaks in the XRD pattern of Cu–Ru/ZrO_2–SO_3–SiO_2 (Fig. 1a), which is due to well dispersion or small particle size of metallic particles [33]. Fig. 1b show that the intensity of peaks at 24.04°, and 28.08° gradually increased with the increase of reduced temperature, indicated the increase of the interaction between SiO_2 and ZrO_2 and the crystallinity of SiO_2 at higher temperature. Fig. S1 shows the XRD patterns of the monometallic oxide supports (SiO_2 and ZrO_2) and Cu–Ru/SiO_2 and Cu–Ru/ZrO_2 catalyst. Three obvious diffraction peaks at 36.72°, 42.36°, and 44.2°, indexed to the Cu_2O and Ru species, can be observed in the SiO_2 supported catalyst. Meanwhile, no obvious Cu or Ru diffraction peaks presented in the XRD pattern of Cu–Ru/ZrO_2 catalyst, indicating that loaded metal species dispersed better on the ZrO_2 support than SiO_2 support. Compared to Cu–Ru/SiO_2 and Cu–Ru/ZrO_2, the active metal particles (Cu and Ru) of Cu–Ru/ZrO_2–SO_3–SiO_2 dispersed better, which may provide the more excellent catalytic hydrogenation activity.

The morphology of as-prepared catalysts was characterized by TEM and the images are shown in Fig. 2. The dark spotted areas presented on all catalysts corresponding to the loaded metallic nanoparticles and their size distributions are inserted in the corresponding TEM images. The average particles sizes were around 5.0 nm for both monometallic catalysts Cu/ZrO_2–SO_3–SiO_2-450 and Ru/ZrO_2–SO_3–SiO_2-450 (Fig. 2a and b) and the average particles sizes were around 7.0 ± 0.5 nm in Fig. 2c and d (Cu–Ru/SiO_2 and Cu–Ru/ZrO_2). Compared to the above two types of catalysts, the bimetallic catalysts on the bimetallic oxides support Cu–Ru/ZrO_2–SO_3–SiO_2-450 presented the lowest particle size of about 3.5 nm (Fig. 2f). As displayed in Fig. 2e, f, and 2h, it can be found that the nanoparticles of Cu–Ru/ZrO_2–SO_3–SiO_2-350 aggregated and the average particles size was about 5.0 nm. When the reduction temperature increased to 450 °C, the average particles size of the catalyst (Cu–Ru/ZrO_2–SO_3–SiO_2-450) decreased to around 3.5 nm and the nanoparticles exhibited better dispersion, which is beneficial for the hydrogenation reaction [34]. With the reduced temperature further increased to 550 °C, obvious aggregation was observed and the average size of the nanoparticles increased to about 7.5 nm, which might be due to the sintering of metal particle at higher temperatures [35]. Therefore, the reduction temperature would affect the particle size of the catalysts, further affecting the catalytic activity of the catalysts. Based on the above results, three important pieces of information could be suggested: 1) the bimetallic oxides support ZrO_2–SO_3–SiO_2 is more conducive to the dispersion of active metals than monometallic support ZrO_2 and SiO_2; 2) The synergy of the copper-ruthenium bimetal is favor in the dispersion of active sites on the support; 3) The reduction temperature would significantly effect the dispersity and particle size of the active metals. Besides, the HRTEM images of Cu–Ru/ZrO_2–SO_3–SiO_2-450 (Fig. 2g) presented that the lattice space of 0.206 nm assigned to the Ru (101) plane and the lattice spaces of 0.207 and 0.200 nm, corresponding to the Cu (111) and Cu_2O (111) plane, respectively [5,36]. These results further indicated that the metal sites were reduced during the preparation process.

The N_2 adsorption-desorption isotherms and pore size distribution curves of the catalysts were exhibited in Fig. 3. All the samples display a type-IV isotherm with H3 hysteresis loop (Fig. 3a and c), suggesting the mesoporous structure of the catalysts [37]. The textural properties of the catalysts are summarized in Table 2. The specific surface area, the pore volume and average pore size of the pristine ZrO_2–SO_3–SiO_2 support are 128.4 m^2/g, 0.13 cm^3/g, 3.99 nm, respectively. The parameters of ZrO_2–SO_3–SiO_2-400 support slightly increased (140.3 m^2/g, 0.14 cm^3/g, and 4.09 nm, respectively), which should be attributed to the removal of impurity in pore. The specific surface area of the catalysts decreased after the metal Cu and Ru loaded, indicating the successfully anchoring of metallic particles. It is worthwhile pointing out that the catalyst also exhibited mesoporous structures (Fig. 3b), which could be conducive to the mass transfer of the reactants during the hydrogenation reaction process [38]. Besides, Cu–Ru/SiO_2 and Cu–Ru/ZrO_2 also exhibited mesoporous structures, while porous structure of these was tanglesome.

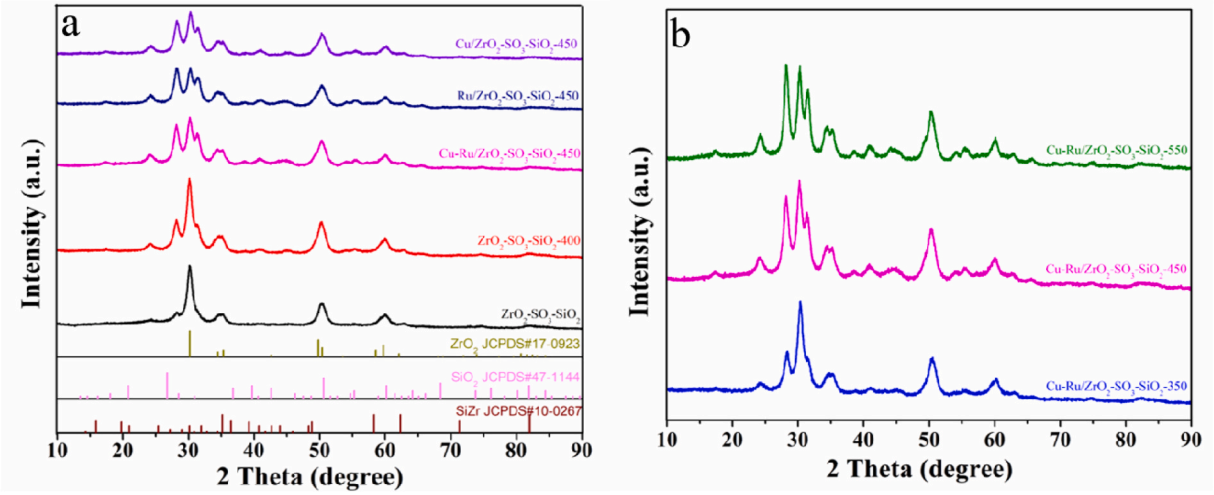

Fig. 1. XRD patterns of as-synthesized catalysts.

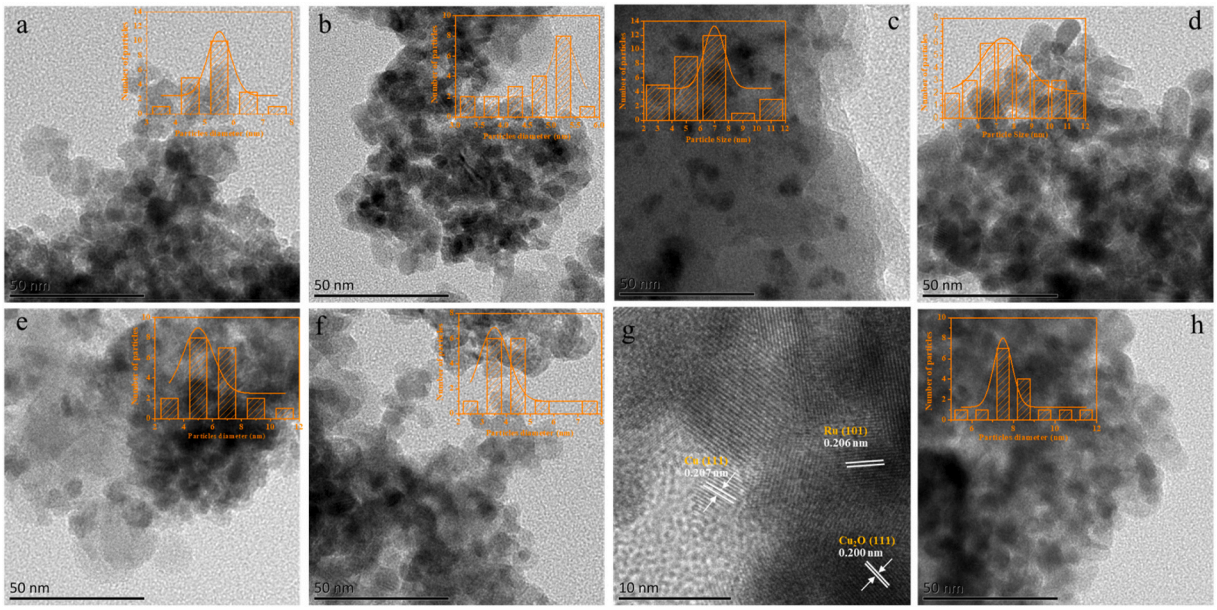

Fig. 2. TEM images and particle size distributions of the as-synthesized catalysts. a: $Cu/ZrO_2–SO_3–SiO_2$-450; b: $Ru/ZrO_2–SO_3–SiO_2$-450; c: Cu–Ru/SiO_2; d: Cu–Ru/ZrO_2; e: Cu–Ru/$ZrO_2–SO_3–SiO_2$-350; f: Cu–Ru/$ZrO_2–SO_3–SiO_2$-450; g: HRTEM of Cu–Ru/$ZrO_2–SO_3–SiO_2$-450; h: Cu–Ru/$ZrO_2–SO_3–SiO_2$-550.

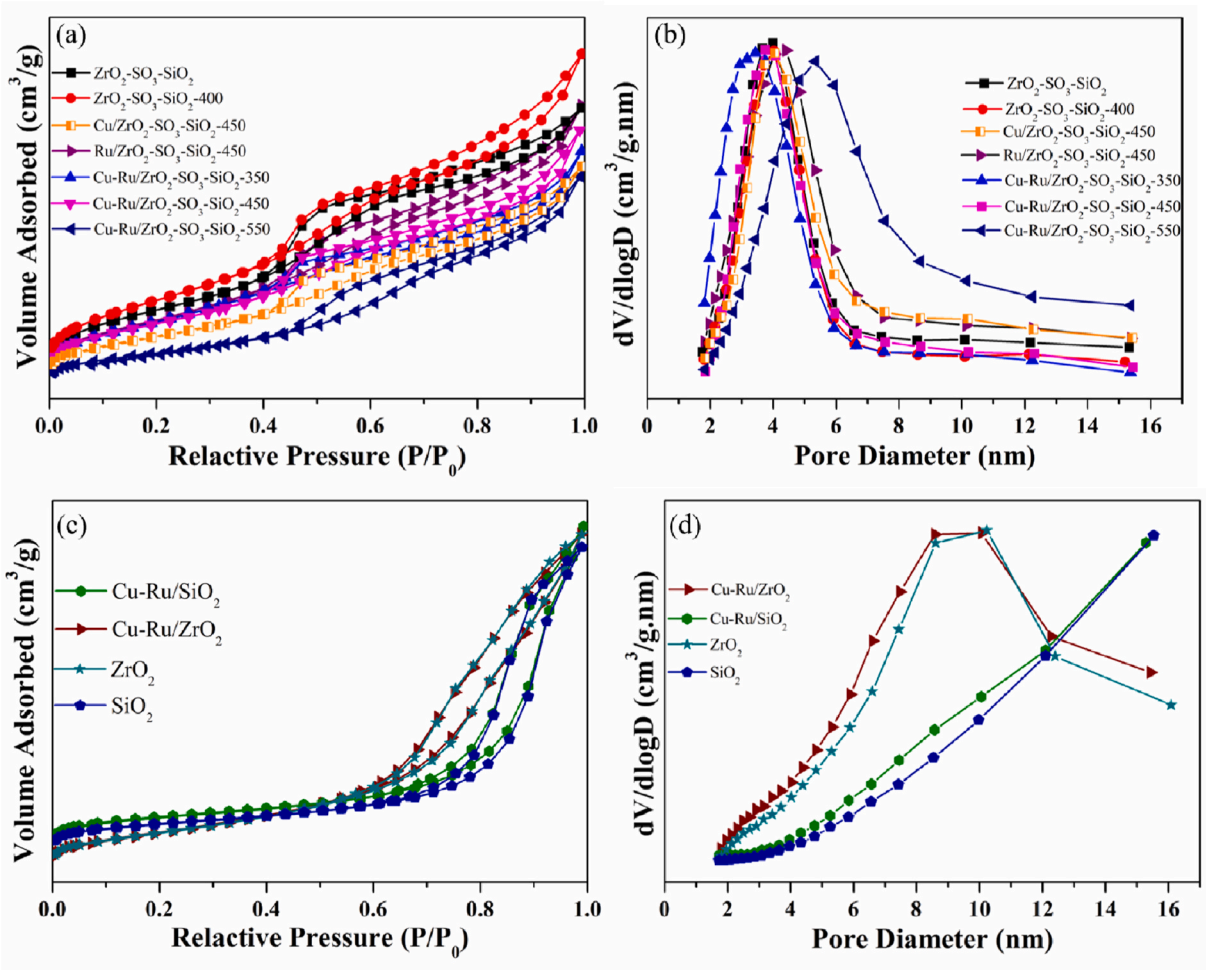

Fig. 3. N_2 ad/desorption isotherm ((a), (c)) and pore diameter distribution ((b), (d)) of the as-synthesized catalysts.

Table 2
Textural Properties of the as-synthesized Catalysts.

Entry	Catalysts	S_{BET} (m^2/g)[a]	V_p (cm^3/g)[b]	D_p (nm)[c]	Acidity (μmol/g)		
					weak	medium	total
1	ZrO_2–SO_3–SiO_2	128.4	0.13	3.99	0.46	0.41	0.87
2	ZrO_2–SO_3–SiO_2-400	140.3	0.14	4.09	0.45	0.34	0.79
3	Cu/ZrO_2–SO_3–SiO_2-450	89.8	0.10	4.35	–	–	–
4	Ru/ZrO_2–SO_3–SiO_2-450	119.0	0.12	4.17	–	–	–
5	Cu–Ru/ZrO_2–SO_3–SiO_2-350	102.8	0.10	3.79	0.65	0.39	1.04
6	Cu–Ru/ZrO_2–SO_3–SiO_2-450	103.3	0.11	4.17	0.45	0.36	0.81
7	Cu–Ru/ZrO_2–SO_3–SiO_2-550	71.2	0.09	5.14	0.46	0.37	0.83
8	ZrO_2	119.2	0.22	7.38	–	–	–
9	SiO_2	196.1	0.73	8.68	–	–	–
10	Cu–Ru/ZrO_2	103.7	0.18	6.99	–	–	–
11	Cu–Ru/SiO_2	179.0	0.38	8.39	–	–	–

[a] BET surface area.
[b] Total pore volume.
[c] Average pore size.

The XPS analysis was conducted to further investigate the chemical state of the metallic sites and interaction between the active sites and support, as shown in Fig. 4 and Fig. S2. The Si 2p spectra of ZrO_2–SO_3–SiO_2 and Cu–Ru/ZrO_2–SO_3–SiO_2 catalysts (Fig. S2a) showed the chemical state no change during the calcination process. Notably, when the metal loaded on the ZrO_2–SO_3–SiO_2 support, the binding energy of Si shifted toward to low field, attributed to the strong interaction between metal particles and support [39]. The binding energy of Zr 3d (Fig. 4a) shifted to a low field after calcination, which may be due to the removal of oxygen in the structure of support. Notably, the binding energy of Zr 3d further shifted to a low field when the Ru particles loaded, which indicated that the Zr atoms may interact with the Ru sites. In Fig. 4a, it can be seen that the binding energy of Zr 3d shifted to high filed, comparison with the Ru/ZrO_2–SO_3–SiO_2-450 catalyst, which may be due to Cu atoms provided the electron to the support and Ru sites. In a word, all bimetallic Cu–Ru catalysts showed the change of binding

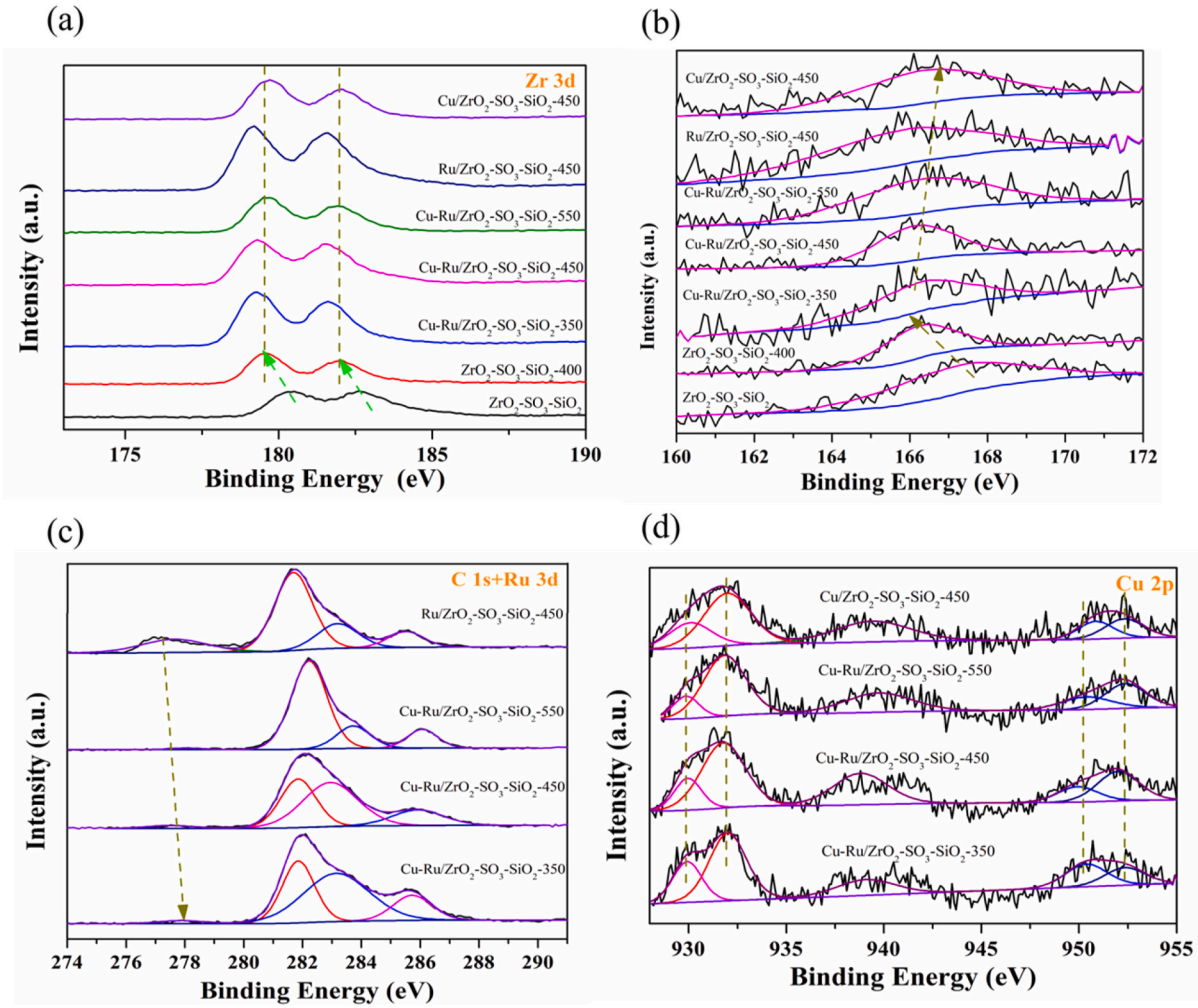

Fig. 4. XPS spectra of as-synthesized catalysts. a: Zr 3d, b: S 2p, c: C 1s and Ru 3d, d: Cu 2p.

energy of Si and Zr atoms, which verified the introduction of secondary metal could enhance the interaction of metallic particles with support. Additionally, the S 2p spectra of samples were analyzed, as shown in Fig. 4b. It can be seen that the binding energy of S 2p shifted to the low field after calcination, due to the removal of oxygen. The binding energy S species shifted toward to high field when the Cu, Ru metal loaded, which suggested the electron transferred from S atoms to the metal sites, promoting the formation of electron-rich active metal sites. The electron-rich active metal sites could enhance the hydrogenation activity of the bimetallic catalyst [40].

The XPS spectra of C 1s and Ru 3d were displayed in Fig. 4c. The binding energy of Ru^0 of the bimetallic Cu–Ru/ZrO_2–SO_3–SiO_2 catalyst shifted to a high field, suggesting the electron transferred from Ru to Cu atoms, which verified interaction of the Cu and Ru sites. Despite this, the S species in the ZrO_2–SO_3–SiO_2 support could donated electron to the metal sites, which could facilitate the dissociation of active hydrogen from hydrogen donors, thus promoting the hydrogenation activity of the catalyst. The XPS spectra of Cu 2p (Fig. 4d) could deconvoluted into five individual peaks around 930.0 eV, 932.0 eV, 939.1 eV, 950.4 eV and 952.3 eV. It can be seen that a doublet Cu $2p_{3/2}$ peaks presented at 930.0 and 932.0 eV and a doublet Cu $2p_{1/2}$ observed at 950.4 eV and 952.3 eV with a binding energy difference between the Cu $2p_{3/2}$ and Cu $2p_{1/2}$ doublets of approximately 20.4 eV [41]. This result indicated the part of Cu^{2+} species was reduced to Cu^0/Cu^+ species during the reduction process [42]. In a word, the heteroatoms of support and bimetal effect could tune the electron distribution of catalytic sites, which would provide the excellent activity.

The acidic property of catalysts could affect the activation of the C═O and C–O of the reactants. Hence, the ZrO_2–SO_3–SiO_2 support and as-prepared catalysts were subjected by NH_3-TPD analysis (Fig. 5a and Table 2). All samples displayed two adsorption peaks at about 140 and 380 °C, indexing to the weak and medium acidic sites of the catalysts, respectively. In addition, the Cu–Ru/ZrO_2–SO_3–SiO_2 catalysts exhibited similar acidity with that of the ZrO_2–SO_3–SiO_2 (Table 2), suggesting that the acidity of the metal loaded catalysts was mainly originated from the ZrO_2–SO_3–SiO_2 support.

The temperature-programmed reduction of hydrogen (H_2-TPR) curves of as-prepared catalysts were displayed in Fig. 5b. Two distinct peaks at around 305 and 642 °C were observed in the Ru/ZrO_2–SO_3–SiO_2 catalyst, whose were higher than these of literatures reported [43,44]. This result may be due to the stronger interaction with ZrO_2–SO_3–SiO_2 support. When the secondary Cu species was introduced, the reduction temperature of the bimetallic catalysts decreased, compared with the monometallic Ru catalyst, indicated that more Ru metal sites were activated by the introducing of the secondary metal Cu. Besides, the Cu–Ru/ZrO_2–SO_3–SiO_2-450 catalyst showed lower reduction temperature than that of Cu–Ru/ZrO_2–SO_3–SiO_2-350, which indicated that more metal sites were reduced at the higher reduction temperature. However, the reduction peaks of catalyst Cu–Ru/ZrO_2–SO_3–SiO_2-550 in the H_2-TPR profile shifted to a higher temperature field, which might be attributed to the formation of larger nanoparticles at higher temperature [45].

3.2. Catalytic transfer hydrogenation of EL to GVL

The catalytic activity of as-prepared catalysts was evaluated in the CTH reaction of EL using 2-PrOH as the reaction solvent as well as the hydrogen donor (Table 3). The pristine ZrO_2–SO_3–SiO_2 support showed limited activity of only 1.8 % GVL yield and 6.5 % EL conversion (Table 3, entry 1). The monometallic catalyst Ru/ZrO_2–SO_3–SiO_2 exhibited higher hydrogenation activity than Cu/ZrO_2–SO_3–SiO_2 (Table 3, entries 2 and 3), suggesting that the metal sites of the catalysts played a crucial role, meanwhile, the effect of Ru sites on the catalytic activity of the catalyst is greater than that of Cu sites in the EL hydrogenation reaction. The Cu–Ru/ZrO_2 provided much higher EL conversion and GVL yield than Cu–Ru/SiO_2 (Table 3, entries 4 and 5),

Table 3
The conversion of EL and GVL yield over different catalysts.

Entry	Substrate	Catalyst	GVL (%)	Conv. (%)
1	EL	ZrO_2–SO_3–SiO_2	1.8	6.5
2	EL	Cu/ZrO_2–SO_3–SiO_2-450	63.8	69.6
3	EL	Ru/ZrO_2–SO_3–SiO_2-450	83.4	90.2
4	EL	Cu–Ru/SiO_2	0.3	0.9
5	EL	Cu–Ru/ZrO_2	83.2	98.4
6	EL	Cu–Ru/ZrO_2–SiO_2	16.4	21.5
7	EL	Cu–Ru/ZrO_2–SO_3–SiO_2-350	72.6	74.7
8	EL	Cu–Ru/ZrO_2–SO_3–SiO_2-450	100	100
9	EL	Cu–Ru/ZrO_2–SO_3–SiO_2-550	83.5	87.5
10[a]	EL	Cu/ZrO_2–SO_3–SiO_2-450+Ru/ZrO_2–SO_3–SiO_2-450	46.2	52.6
11[b]	EL	Cu–Ru/ZrO_2–SO_3–SiO_2-450	96.0	96.9
12[c]	EL	Cu–Ru/ZrO_2–SO_3–SiO_2-450	96.9	97.8
13[d]	EL	Cu–Ru/ZrO_2–SO_3–SiO_2-450	95.7	100

Reaction conditions: EL 1 mmol, catalyst 100 mg, 2-PrOH 5 mL, 180 °C, 12 h, N_2. [a]mixture of Ru/ZrO_2–SO_3–SiO_2-450 and Cu/ZrO_2–SO_3–SiO_2-450, [b]5 wt % H_2O added, [c]conducted in the air, [d]catalyst 60 mg 24 h.

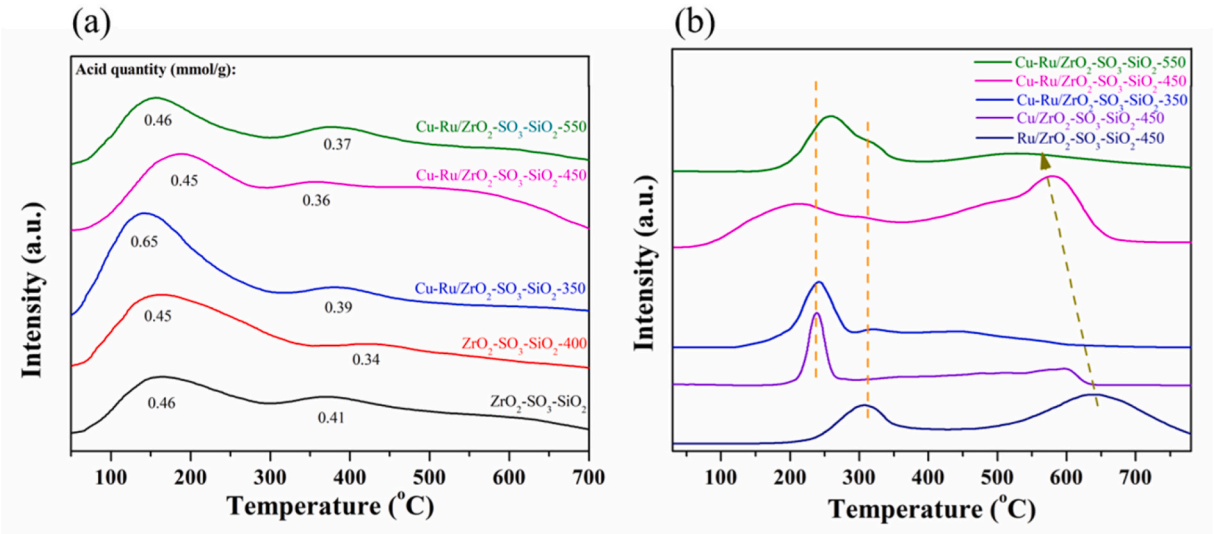

Fig. 5. NH_3-TPD (a) and H_2-TPR (b) spectrum of the as-synthesized catalysts.

indicating that ZrO_2 showed a more active role than SiO_2 in this hydrogenation system. This result could be attributed to the stronger electronic effect and interaction between the metallic sites and the ZrO_2 support, which was confirmed by results of XRD and XPS characterization. Meanwhile, the Cu–Ru/ZrO_2–SiO_2 catalyst exhibited the 21.5 % EL conversion and 16.4 % GVL yield (Table 3, entry 6). Notably, the bimetallic Cu–Ru catalysts prepared at the different reduction temperature exhibited different catalytic activity, the Cu–Ru/ZrO_2–SO_3–SiO_2-350 catalyst provided 74.7 % EL conversion and 72.6 % GVL yield (Table 3, entry 7), while the reduction temperature increased to 450 °C, the catalyst achieved a full EL conversion and a theoretical GVL yield (100 %) (Table 3, entry 8). This result corresponded to a more sufficient reduction of metal sites, higher metal dispersion, and smaller metal particle size [46,47]. With the reduction temperature further increased to 550 °C, the catalytic hydrogenation activity of Cu–Ru/ZrO_2–SO_3–SiO_2-550 decreased down to 83.5 % of GVL yield (Table 3, entry 9), which was due to the aggregation of metal particles at high treatment temperature [48]. It can be seen that the ZrO_2–SO_3–SiO_2 support showed the excellent performance than that of the SiO_2, ZrO_2, and ZrO_2–SiO_2 supports, which indicated that the S played an important role in the hydrogenation reaction.

Besides, to verify the synergy effect of Cu and Ru sites on Cu–Ru/ZrO_2–SO_3–SiO_2, the Cu/ZrO_2–SO_3–SiO_2 and Ru/ZrO_2–SO_3–SiO_2 were physically mixed and subjected to the hydrogenation reaction, which showed a lower GVL yield (Table 3, entry 10) than bimetallic Cu–Ru/ZrO_2–SO_3–SiO_2 catalyst. This result suggested that the synergy of bimetallic Cu–Ru sites could effectively enhance the hydrogenation activity of the catalyst. In addition, the H_2O and air would affect the catalytic efficiency in the hydrogenation system. Subsequently, the effect of the H_2O and air was investigated in hydrogenation reaction of EL. The 96.0 % and 96.9 % of GVL yield was achieved over the Cu–Ru/ZrO_2–SO_3–SiO_2-450 catalyst, when the hydrogenation reaction was conducted in the 5 *wt*% H_2O system and air condition, respectively, (Table 3, entry 11 and 12). Based on the above experimental results, the Cu–Ru/ZrO_2–SO_3–SiO_2-450 exhibited the high catalytic activity and stability in the hydrogenation system.

The reaction temperature has a profound effect on the reaction rate. Hence, the hydrogenation of EL was performed at a range from 120 to 200 °C (Fig. 6a). When the reaction proceeded at a milder condition (120 °C), only 20.3 % GVL yield was achieved with 20.6 % EL conversion. With the increase of reaction temperature, the EL conversion and GVL yield gradually increased until a maximum GVL yield of 100 % obtained at 180 °C, which was attributed to the fact that higher temperature promotes the dissociation of active hydrogen ([H]), thus enhancing the reaction efficiency of EL hydrogenation reaction [19]. While the reaction temperature further increased to 200 °C, the GVL yield slightly decreased to 91.7 %, which may be due to the polymerization of reactant, intermediates, and products at high reaction temperature [49]. Furthermore, the influence of reaction time was explored in Fig. 6b. The EL conversion and GVL yield increased apparently with the extension of reaction time, and the maximum GVL yield was achieved at 12 h. While the reaction time further prolonged, the GVL yield decreased slightly, which might be owing to the side-reactions. Additionally, the influence of catalyst dosage in the hydrogenation system was evaluated (Fig. 6c). Only 42.7 % EL conversion and 40.7 % GVL yield were achieved with 40 mg Cu–Ru/ZrO_2–SO_3–SiO_2-450 catalyst. As the catalyst dosage gradually increased, both EL conversion and GVL yield increased and the maximum GVL yield was obtained at 100 mg of Cu–Ru/ZrO_2–SO_3–SiO_2-450 catalyst. When the catalyst dosage further increased to 120 mg, the EL conversion remained, while the GVL yield decreased slightly, which may be due to the side-reactions suffered on excessive active metal sites of the catalyst [50]. Noteworthy, the conversion of EL to GVL reaction could conduct well with a lower catalyst dosage by prolonging the reaction time. For instance, the hydrogenation of EL to GVL with 60 mg of catalyst dosage provided 95.7 % GVL yield when the reaction time extending the reaction time to 24 h (Table 3, entry 13), which further indicated the high hydrogenation activity (EL to GVL) of Cu–Ru/ZrO_2–SO_3–SiO_2-450 catalyst.

The effect of different H-donor solvent on the hydrogenation reaction was investigated at the optimal reaction conditions (Table 4). The experimental results presented that primary alcohols (methanol and ethanol) provided poor performance as H-donor solvent in the hydrogenation reaction (Table 4, entries 1 and 2), which was ascribed to the more difficult β-hydride elimination when primary alcohol formed alkoxy species on the surface of the catalyst [19,51]. The secondary alcohols (including 2-PrOH, 2-BuOH, and 3-Pentanol) provided excellent performance in the reaction. Specifically, 100 %, 91.7 % and 87.0 % GVL yield was obtained in the 2-PrOH, 2-BuOH and 3-Pentanol solvent, respectively. The difference on the hydrogenation performance of three secondary solvents could be attributed to difference of the reduction potential of the reductive alcohols [29]. In a word, the secondary alcohols exhibited the more outstanding performance than that of primary alcohols.

As we know, the adsorption and desorption of reactants and products on the surface of catalysts could affect the reaction rate in heterogeneous catalytic system [52]. Thus, the adsorption experiments were conducted and the test results of different catalysts in the hydrogenation system

Table 4
CTH reaction of EL in Different H-Donor Solvent[a].

Entry	Substrate	Solvent	GVL (%)	Conv. (%)
1	EL	MeOH	32.9	34.1
2	EL	EtOH	11.2	12.1
3	EL	2-PrOH	100	100
5	EL	2-BuOH	91.4	94.6
6	EL	3-Pentanol	87.0	90.5

[a] Reaction conditions: EL 1 mmol, catalyst 100 mg, 2-PrOH 5 mL, 180 C, 12 h, N_2.

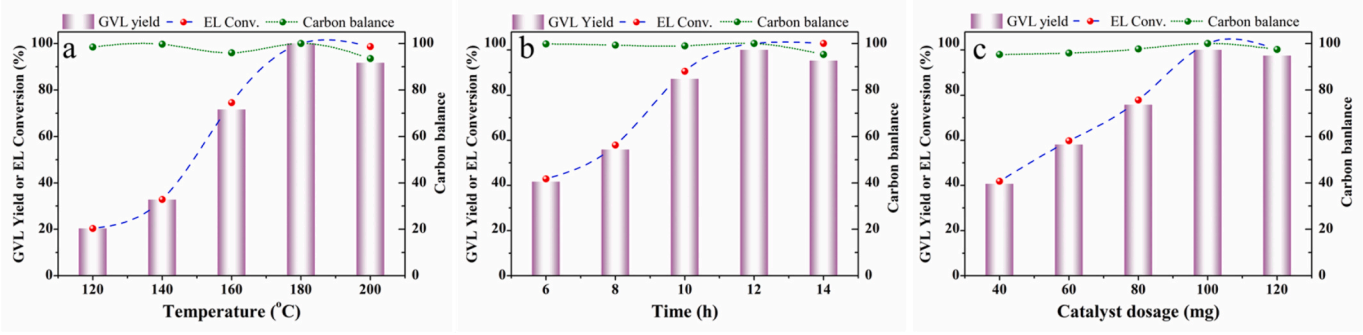

Fig. 6. Influences of (a) reaction temperature, (b) reaction time, and (c) catalysts dosage on the reaction conversion and yield. Condition: EL 1.0 mmol, catalyst 100 mg, 2-PrOH 5 mL. (a) 12 h; (b) 180 °C.

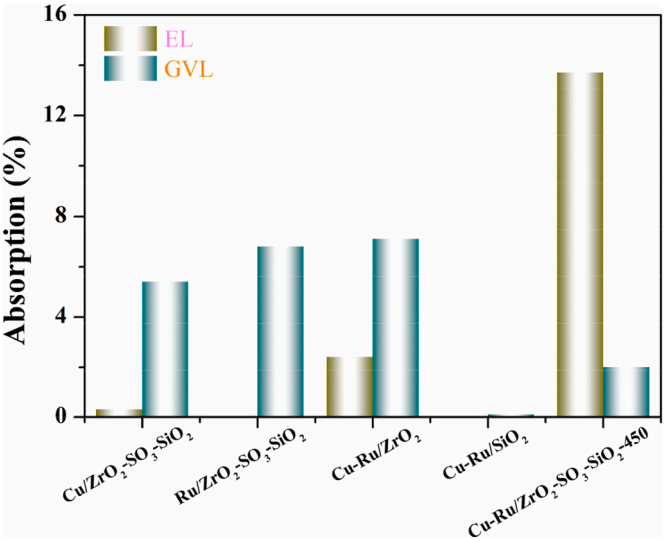

Fig. 7. Adsorption test of reaction substrates EL, product GVL on the different catalysts in the reaction system.

were displayed in Fig. 7. $Cu/ZrO_2–SO_3–SiO_2$ and $Ru/ZrO_2–SO_3–SiO_2$ were favorable to adsorb the product GVL, compared to reactant EL, which would be not beneficial for desorption of GVL product and release of active sites, thus inhibiting the reaction rate. $Cu–Ru/ZrO_2$ catalyst shows a similar result with that of $Cu/ZrO_2–SO_3–SiO_2$ catalyst. $Cu–Ru/SiO_2$ performed poor adsorption capacity of EL and GVL, thus this catalyst presented a poor hydrogenation performance (0.3 % of GVL yield, 0.9 % of EL conversion). Notably, the $Cu–Ru/ZrO_2–SO_3–SiO_2$-450 exhibited the excellent absorption performance of EL and desorption performance of GVL. This result supported it the excellent performance on the conversion of EL and yield of GVL. Meanwhile, GVL could efficiently desorb from the surface of $Cu–Ru/ZrO_2–SO_3–SiO_2$-450, thus releasing the catalytic active sites for sequential reactions. The adsorption experimental results indicated the excellent affinity between the substrate EL and the $Cu–Ru/ZrO_2–SO_3–SiO_2$-450, which could enhance the hydrogenation reaction.

To further estimate the catalytic activity of $Cu–Ru/ZrO_2–SO_3–SiO_2$-450 catalyst in the hydrogenation system, the kinetics of conversion of EL to GVL was investigated. EL conversion at the different temperatures over the bimetallic Cu–Ru catalyst were traced, as shown in Fig. 8. The apparent activation energy (E_a) of EL hydrogenation to GVL was calculated by the Arrhenius equation $k = Ae^{(-Ea/RT)}$. The apparent activation energy for EL conversion was determined to be 67.8 kJ/mol.

3.3. Stability of $Cu–Ru/ZrO_2–SO_3–SiO_2$-450 catalyst

The reusability of catalyst is a crucial factor of heterogeneous catalysts, determining the economy and sustainability of the reaction system. Thus, the $Cu–Ru/ZrO_2–SO_3–SiO_2$-450 catalyst was evaluated by performing consecutive runs using the recovered catalyst. Specifically, the $Cu–Ru/ZrO_2–SO_3–SiO_2$-450 catalyst was separated by centrifugation after the hydrogenation reaction and washed with 2-PrOH for three times, then directly subjected to the next run. The EL conversion and GVL yield decreased slightly to 96.5 % and 95.4 % in the fourth run (Fig. 9), while the carbon balance of the reaction remained unchanged. There may be due to the mass loss of catalyst during the recycling process. Besides, the hydrogenation reaction over $Cu–Ru/ZrO_2–SO_3–SiO_2$-450 catalyst was carried out at 160 °C to further test its reusability (Fig. S3). The results presented that the EL conversion and GVL yield remained during the recycling experiment, suggesting the $Cu–Ru/ZrO_2–SO_3–SiO_2$-450 could keep high activity and stability in the EL hydrogenation reaction.

To further investigate the stability of $Cu–Ru/ZrO_2–SO_3–SiO_2$-450, the catalyst after the fifth run was collected and directly characterized (Fig. 10). The XRD spectra of fresh and recovered catalyst presented similar diffraction peaks (Fig. 10a), suggested the metallic sites on the surface of catalyst were stable during the hydrogenation reaction. The TEM image of the recovered $Cu–Ru/ZrO_2–SO_3–SiO_2$-450 catalyst (Fig. 10b) displayed no obvious aggregation of metallic particles, which is consistent with the XRD result. Besides, the XPS analysis (C 1s + Ru 3d and Cu 2p) of recovered catalysts were conducted to analyze the change of active sites (Fig. 10c and d). It can be seen that the reduced Ru^0 and

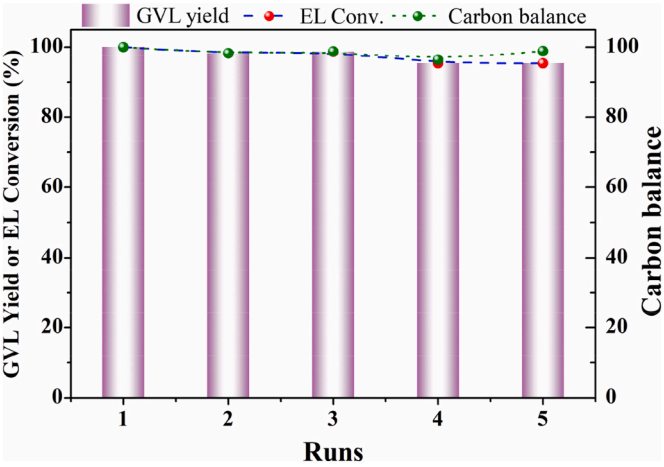

Fig. 9. Performance of recycled Ru/UCN catalyst. Conditions: EL 1.0 mmol, catalyst 100 mg, 2-PrOH 5 mL, 180 °C, 12 h.

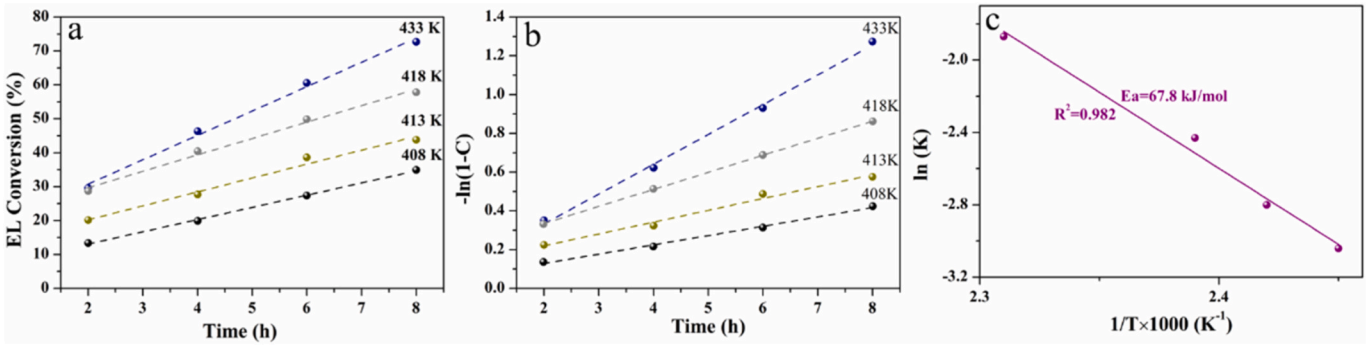

Fig. 8. (a) Time-course plots of the rate-determining step of EL hydrogenation over $Cu–Ru/ZrO_2–SO_3–SiO_2$ catalyst at 413−433 K temperature, respectively. (b) –ln (1−C) vs reaction time plots. (c) Arrhenius plots of the rate-determining step. Reaction condition: EL 1 mmol, $Cu–Ru/ZrO_2–SO_3–SiO_2$ 100 mg, 2-PrOH 5 mL.

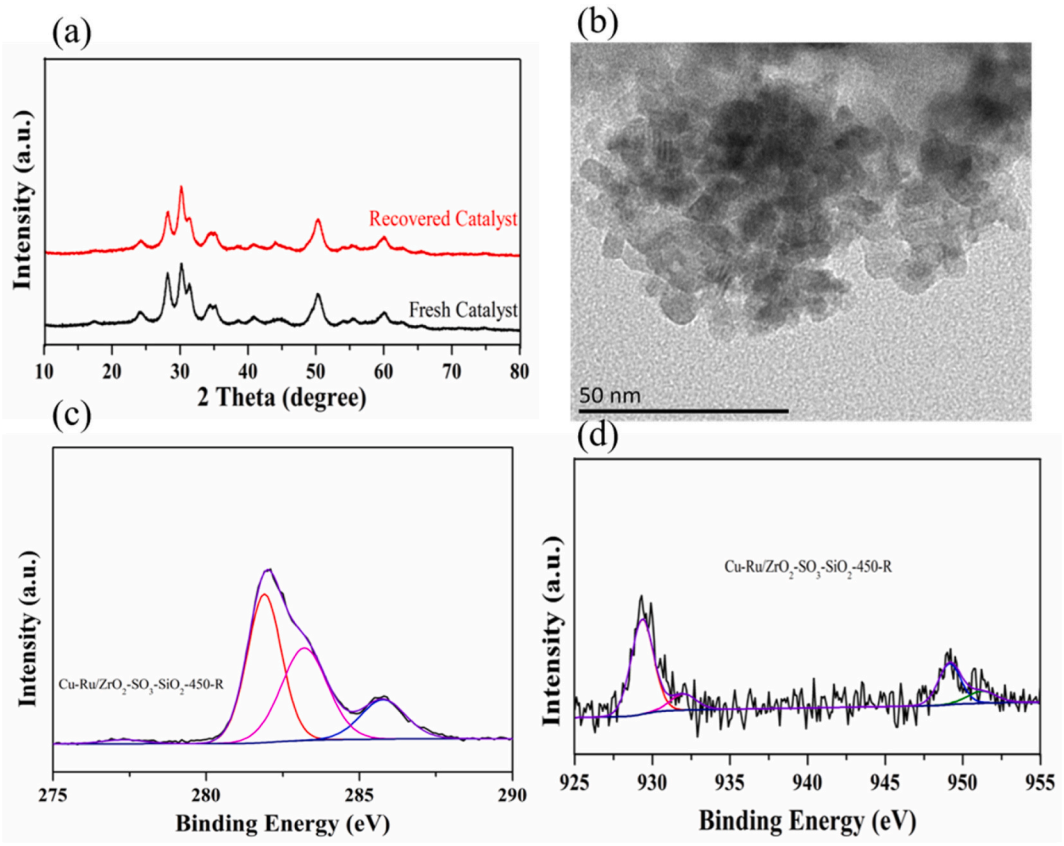

Fig. 10. XRD characterization (a), TEM image (b), XPS analysis (c) of recovered Cu–Ru/ZrO_2–SO_3–SiO_2-450 catalyst after 5th cycle.

Cu^0 were detected, which could provide hydrogenation sites for the EL conversion. The above characterization results further demonstrated the outstanding stability and recyclability of Cu–Ru bimetallic catalyst in the CTH reaction system.

Table 5
Substrate scope of Cu–Ru/ZrO_2–SO_3–SiO_2-450 catalyzed hydrogenation reaction[a].

Entry	Substrate	Product	GVL (%)	Conv. (%)
1			46.3	71.4
2			99.9	100
3			83.3	87.6
4			94.1	100
5	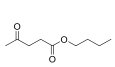		> 99	100
6			> 99	100
7		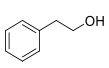	> 99	100

[a] Reaction conditions: substrate 1 mmol, Cu–Ru/ZrO_2–SO_3–SiO_2 100 mg, 2-PrOH 5 mL, 180 C, 12 h, N_2.

3.4. Hydrogenation of different biomass-derived substrate

Finally, the Cu–Ru/ZrO_2–SO_3–SiO_2-450 catalyst was tested for hydrogenation of several typical biomass-derived platform compounds including levulinic acid (LA), levulinate esters, furfural, benzaldehyde, phenylacetaldehyde and acetophenone (Table 5). For levulinic acid, only 46.3 % GVL yield and 71.4 % LA conversion were achieved (Table 5, entry 1), which may be due to the metal sites of the catalyst would be etched in the acidic medium [22]. It can be seen that 99.9 % and 83.3 % GVL yields were obtained, corresponding to methyl levulinate and butyl levulinate as the substrate, respectively (Table 5, entries 2 and 3), indicating the catalyst exhibited excellent hydrogenation activity of levulinate esters. The different catalytic performance of this catalyst on the different levulinate esters might be attributed to the steric hindrance of the alkyl groups [29]. Furfural, a typical hemicellulose-derived compound, could be selectively converted to furfural alcohol over the Cu–Ru/ZrO_2–SO_3–SiO_2-450 catalyst, and 94.1 % yield of furfural alcohol was obtained (Table 5, entry 4). Additionally, the hydrogenation activity of the bimetallic Cu–Ru catalyst was also evaluated on the lignin-derived compounds including benzaldehyde, phenylacetaldehyde and acetophenone. The experimental results presented the high catalytic activity for the selective hydrogenation of C═O bonds (yield of products > 99 %). Notably, these results indicated the Cu–Ru/ZrO_2–SO_3–SiO_2-450 catalyst could selectively convert the C═O bond, while ignoring carbon-carbon unsaturated bonds. Thus, it can be widely applied to the selective hydrogenation of biomass-derived substrates with C═O bond.

4. Conclusion

In this study, a series of bimetallic Cu–Ru catalysts were prepared and applied to the selective hydrogenation reaction of the biomass-

derived carbonyl compounds. The characterization results of as-prepared bimetallic catalysts showed that the particle size, dispersion, and electron states of metal sites could be affected by the support. Notably, the electrons could transfer from S heteroatom to the metal sites to form the electron-rich Cu and Ru species, which could provide high hydrogenation activity in the CTH reaction system. Besides, the reduction temperature performed an important effect for the physico-chemical properties of catalyst. And the experimental results indicated that Cu–Ru/ZrO_2–SO_3–SiO_2-450 presented higher hydrogenation activity toward the CTH reaction of EL to GVL with a theoretical yield at the optimal reaction conditions. Meanwhile, the Cu–Ru bimetallic catalyst exhibited high stability and reusability, and could provide more than 95 % GVL yield after 5 reaction runs. Besides, the Cu–Ru/ZrO_2–SO_3–SiO_2-450 catalyst exhibited high catalytic hydrogenation activity for a variety of biomass-derived carbonyl compounds to produce corresponding alcohols. In a word, the bimetallic Cu–Ru/ZrO_2–SO_3–SiO_2-450 was efficient catalyst for the selective hydrogenation of biomass-derived platform compounds unsaturation C═O bond. This work could provide a new insight for design the efficient catalyst using the interaction between the active sites and the support.

CRediT authorship contribution statement

Bo Cai: Investigation, Writing – original draft, preparation. **Rui Kang:** Visualization, Software. **Junfeng Feng:** Visualization, Software. **Thomas L. Eberhardt:** Writing- Reviewing. **Zhongqing Ma:** Writing-Reviewing. **Qingge Zhu:** Visualization, Software. **Hui Pan:** Conceptualization, Supervision, Writing – review & editing.

Declaration of competing interest

The authors declare that they have no known competing financial interests or personal relationships that could have appeared to influence the work reported in this paper.

Acknowledgments

The study was supported by the International Joint Research Center for Biomass Materials, (Southwest Forestry University) (No. 2022-GH002) and Supported by the 111 Project (D21027), and the Research Foundation of Talented Scholars of Zhejiang A & F University (2022LFR073).

Appendix A. Supplementary data

Supplementary data to this article can be found online at https://doi.org/10.1016/j.renene.2023.119833.

References

[1] Y. Liang, H. Wang, H. Xin, X. Hu, L. Yan, Q. Zhang, C. Wang, Q. Liu, L. Ma, Selective cellulose hydrogenolysis to 2,5-hexanedione and 1-Hydroxy-2-hexanone using Ni@NC combined with H3PO4, ACS Sustain. Chem. Eng. 9 (2021) 15394–15405, https://doi.org/10.1021/acssuschemeng.1c03858.

[2] J. Luo, G. Gong, C. Cui, S. Sun, J. Lin, R. Ma, J. Sun, Microwave-induced one-pot preparation of bifunctional N-Fe/BC catalysts and oriented production of phenol-enriched bio-oil from biomass pyrolysis: catalyst synthesis, performance evaluation, and mechanism insight via theoretical calculations, ACS Catal. 12 (2022) 11318–11339, https://doi.org/10.1021/acscatal.2c01841.

[3] A. Wang, T. Zhang, One-Pot conversion of cellulose to ethylene glycol with multifunctional tungsten-based catalysts, Acc. Chem. Res. 46 (2013) 1377–1386, https://doi.org/10.1021/ar3002156.

[4] R.S. de Almeida Ribeiro, L.E. Monteiro Ferreira, V. Rossa, C.G.S. Lima, M. W. Paixão, R.S. Varma, T. de Melo Lima, Graphitic carbon nitride-based materials as catalysts for the upgrading of lignocellulosic biomass-derived molecules, ChemSusChem (2020) 1–14, https://doi.org/10.1002/cssc.202001017.

[5] Y.B. Huang, A.F. Liu, Q. Zhang, K.M. Li, W.B. Porterfield, L.C. Li, F. Wang, Mechanistic insights into the solvent-driven adsorptive hydrodeoxygenation of biomass derived levulinate acid/ester to 2-methyltetrahydrofuran over bimetallic Cu-Ni catalysts, ACS Sustain. Chem. Eng. 8 (2020) 11477–11490, https://doi.org/10.1021/acssuschemeng.0c00335.

[6] R. Mariscal, P. Maireles-Torres, M. Ojeda, I. Sádaba, M. López Granados, Furfural: a renewable and versatile platform molecule for the synthesis of chemicals and fuels, Energy Environ. Sci. 9 (2016) 1144–1189, https://doi.org/10.1039/c5ee02666k.

[7] O.A. Abdelrahman, A. Heyden, J.Q. Bond, Analysis of kinetics and reaction pathways in the aqueous-phase hydrogenation of levulinic acid to form γ-valerolactone over Ru/C, ACS Catal. 4 (2014) 1171–1181, https://doi.org/10.1021/cs401177p.

[8] X. Gao, S. Zhu, M. Dong, J. Wang, W. Fan, Ru nanoparticles deposited on ultrathin TiO2 nanosheets as highly active catalyst for levulinic acid hydrogenation to Γ-valerolactone, Appl. Catal. B Environ. 259 (2019), 118076, https://doi.org/10.1016/j.apcatb.2019.118076.

[9] H. Chen, Q. Xu, D. Zhang, W. Liu, X. Liu, D. Yin, Highly efficient synthesis of γ-valerolactone by catalytic conversion of biomass-derived levulinate esters over support-free mesoporous Ni, Renew. Energy 163 (2021) 1023–1032, https://doi.org/10.1016/j.renene.2020.09.023.

[10] Y. Zhao, H. Zhou, W. Chen, Y. Tong, C. Zhao, Y. Lin, Z. Jiang, Q. Zhang, Z. Xue, W. C. Cheong, B. Jin, F. Zhou, W. Wang, M. Chen, X. Hong, J. Dong, S. Wei, Y. Li, Y. Wu, Two-step carbothermal welding to access atomically dispersed pd1 on three-dimensional zirconia nanonet for direct indole synthesis, J. Am. Chem. Soc. 141 (2019) 10590–10594, https://doi.org/10.1021/jacs.9b03182.

[11] J. Wu, C. Liu, Y. Zhu, X. Song, C. Wen, X. Zhang, C. Wang, L. Ma, Understanding the geometric and electronic factors of PtNi bimetallic surfaces for efficient and selective catalytic hydrogenation of biomass-derived oxygenates, J. Energy Chem. 60 (2021) 16–24, https://doi.org/10.1016/j.jechem.2020.12.011.

[12] H. Liu, X. Cao, X. Tang, X. Zeng, Y. Sun, X. Ke, L. Lin, Choline chloride-promoted efficient solvent-free hydrogenation of biomass-derived levulinic acid to γ-valerolactone over Ru/C, Green Chem. 23 (2021) 1983–1988, https://doi.org/10.1039/d1gc00100k.

[13] K.-M. Li, Q. Zhang, Z.-M. Xu, R. Chen, T.-T. Liu, J.-Y. Luo, Y.-W. Wu, Y.-B. Huang, Q. Lu, Tunable mono- and di-methylation of amines with methanol over bimetallic CuCo nanoparticle catalysts, Green Chem. 24 (2022) 5965–5977, https://doi.org/10.1039/D2GC00827K.

[14] M.J. Gilkey, B. Xu, Heterogeneous catalytic transfer hydrogenation as an effective pathway in biomass upgrading, ACS Catal. 6 (2016) 1420–1436, https://doi.org/10.1021/acscatal.5b02171.

[15] R. Huang, Y. Liu, J. Zhang, J. Wei, L. Peng, X. Tang, Catalytic transfer hydrogenation of levulinic acid to γ-valerolactone over an acids-base trifunctional Hf-bagasse coordination complex derived catalyst, Fuel 305 (2021), https://doi.org/10.1016/j.fuel.2021.121557.

[16] T. Tabanelli, E. Paone, P. Blair Vásquez, R. Pietropaolo, F. Cavani, F. Mauriello, Transfer hydrogenation of methyl and ethyl levulinate promoted by a ZrO2 catalyst: comparison of batch vs continuous gas-flow conditions, ACS Sustain. Chem. Eng. 7 (2019) 9937–9947, https://doi.org/10.1021/acssuschemeng.9b00778.

[17] L. Lu, S. Zou, B. Fang, The critical impacts of ligands on heterogeneous nanocatalysis: a review, ACS Catal. 11 (2021) 6020–6058, https://doi.org/10.1021/acscatal.1c00903.

[18] M. Xu, D. Li, K. Sun, L. Jiao, C. Xie, C. Ding, H. Jiang, Interfacial microenvironment modulation boosting electron transfer between metal nanoparticles and MOFs for enhanced photocatalysis, Angew. Chem. 133 (2021) 16508–16512, https://doi.org/10.1002/ange.202104219.

[19] B. Cai, Y. Zhang, J. Feng, C. Huang, T. Ma, H. Pan, Highly efficient g-C3N4 supported ruthenium catalysts for the catalytic transfer hydrogenation of levulinic acid to liquid fuel γ-valerolactone, Renew. Energy 177 (2021) 652–662, https://doi.org/10.1016/j.renene.2021.05.159.

[20] Y. Lu, Y. Wang, Q. Tang, Q. Cao, W. Fang, Synergy in Sn-Mn oxide boosting the hydrogenation catalysis of supported Pt nanoparticles for selective conversion of levulinic acid, Appl. Catal. B Environ. 300 (2022), 120746, https://doi.org/10.1016/j.apcatb.2021.120746.

[21] Y. Cen, S. Zhu, J. Guo, J. Chai, W. Jiao, J. Wang, W. Fan, Supported cobalt catalysts for the selective hydrogenation of ethyl levulinate to various chemicals, RSC Adv. 8 (2018) 9152–9160, https://doi.org/10.1039/c8ra01316k.

[22] B. Cai, X.C. Zhou, Y.C. Miao, J.Y. Luo, H. Pan, Y.B. Huang, Enhanced catalytic transfer hydrogenation of ethyl levulinate to γ-valerolactone over a robust Cu-Ni bimetallic catalyst, ACS Sustain. Chem. Eng. 5 (2017) 1322–1331, https://doi.org/10.1021/acssuschemeng.6b01677.

[23] Y. Tang, J. Fu, Y. Wang, H. Guo, X. Qi, Bimetallic Ni-Zn@OMC catalyst for selective hydrogenation of levulinic acid to γ-valerolactone in water, Fuel Process. Technol. 240 (2023), 107559, https://doi.org/10.1016/j.fuproc.2022.107559.

[24] I. Obregón, E. Corro, U. Izquierdo, J. Requies, P.L. Arias, Levulinic acid hydrogenolysis on Al2O3-based Ni-Cu bimetallic catalysts, Chin. J. Catal. 35 (2014) 656–662, https://doi.org/10.1016/S1872-2067(14)60051-6.

[25] C. Li, G. Xu, Y. Zhai, X. Liu, Y. Ma, Y. Zhang, Hydrogenation of biomass-derived ethyl levulinate into Γ-valerolactone by activated carbon supported bimetallic Ni and Fe catalysts, Fuel 203 (2017) 23–31, https://doi.org/10.1016/j.fuel.2017.04.082.

[26] F. Ye, D. Zhang, T. Xue, Y. Wang, Y. Guan, Enhanced hydrogenation of ethyl levulinate by Pd-AC doped with Nb 2O5, Green Chem. 16 (2014) 3951–3957, https://doi.org/10.1039/c4gc00972j.

[27] M. Kondeboina, S.S. Enumula, V.R.B. Gurram, R.R. Chada, D.R. Burri, S.R. R. Kamaraju, Selective hydrogenation of biomass-derived ethyl levulinate to γ-valerolactone over supported Co catalysts in continuous process at atmospheric pressure, J. Ind. Eng. Chem. 61 (2018) 227–235, https://doi.org/10.1016/j.jiec.2017.12.020.

[28] J.F. Kurisingal, Y. Rachuri, A.S. Palakkal, R.S. Pillai, Y. Gu, Y. Choe, D.-W. Park, Water-tolerant DUT-series metal–organic frameworks: a theoretical–experimental

study for the chemical fixation of CO 2 and catalytic transfer hydrogenation of ethyl levulinate to γ-valerolactone, ACS Appl. Mater. Interfaces 11 (2019) 41458–41471, https://doi.org/10.1021/acsami.9b16834.
[29] X. Tang, H. Chen, L. Hu, W. Hao, Y. Sun, X. Zeng, L. Lin, S. Liu, Conversion of biomass to γ-valerolactone by catalytic transfer hydrogenation of ethyl levulinate over metal hydroxides, Appl. Catal. B Environ. 147 (2014) 827–834, https://doi.org/10.1016/j.apcatb.2013.10.021.
[30] A. Bunrit, T. Butburee, M. Liu, Z. Huang, K. Meeporn, C. Phawa, J. Zhang, S. Kuboon, H. Liu, K. Faungnawakij, F. Wang, Photo-thermo-dual catalysis of levulinic acid and levulinate ester to γ-valerolactone, ACS Catal. 12 (2022) 1677–1685, https://doi.org/10.1021/acscatal.1c04959.
[31] J. Yang, W. Huang, Y. Liu, T. Zhou, Enhancing the conversion of ethyl levulinate to γ-valerolactone over Ru/UiO-66 by introducing sulfonic groups into the framework, RSC Adv. 8 (2018) 16611–16618, https://doi.org/10.1039/c8ra01314d.
[32] N. Ji, X. Diao, Z. Yu, Z. Liu, S. Jiang, X. Lu, C. Song, Q. Liu, D. Ma, C. Liu, Catalytic transfer hydrogenation of ethyl levulinate to γ-valerolactone over supported MoS2catalysts, Catal. Sci. Technol. 11 (2021) 5062–5076, https://doi.org/10.1039/d1cy00524c.
[33] C. Zhang, C. Jia, Y. Cao, Y. Yao, S. Xie, S. Zhang, H. Lin, Water-assisted selective hydrodeoxygenation of phenol to benzene over the Ru composite catalyst in the biphasic process, Green Chem. 21 (2019) 1668–1679, https://doi.org/10.1039/c8gc04017f.
[34] Z. Huang, K.J. Barnett, J.P. Chada, Z.J. Brentzel, Z. Xu, J.A. Dumesic, G.W. Huber, Hydrogenation of γ-butyrolactone to 1,4-butanediol over CuCo/TiO 2 bimetallic catalysts, ACS Catal. 7 (2017) 8429–8440, https://doi.org/10.1021/acscatal.7b03016.
[35] F. Lan, H. Zhang, C. Zhao, Y. Shu, Q. Guan, W. Li, Copper clusters encapsulated in carbonaceous mesoporous silica nanospheres for the valorization of biomass-derived molecules, ACS Catal. 12 (2022) 5711–5725, https://doi.org/10.1021/acscatal.2c01270.
[36] Y.T. Li, S.H. Zhang, G.P. Zheng, P. Liu, Z.K. Peng, X.C. Zheng, Ultrafine Ru nanoparticles anchored to porous g-C3N4 as efficient catalysts for ammonia borane hydrolysis, Appl. Catal. Gen. 595 (2020) 2–9, https://doi.org/10.1016/j.apcata.2020.117511.
[37] V.R. Battula, A. Jaryal, K. Kailasam, Visible light-driven simultaneous H2 production by water splitting coupled with selective oxidation of HMF to DFF catalyzed by porous carbon nitride, J. Mater. Chem. A 7 (2019) 5643–5649, https://doi.org/10.1039/c8ta10926e.
[38] I.Y. Eom, S. Lee, S.Y. Hwang, M. Choi, Versatile post-synthetic Sn incorporation into hierarchically porous BEA zeolite for glucose isomerization in 1-butanol, Microporous Mesoporous Mater. 307 (2020), 110524, https://doi.org/10.1016/j.micromeso.2020.110524.
[39] Q. Liu, L. Ai, J. Jiang, MXene-derived TiO 2 @C/g-C 3 N 4 heterojunctions for highly efficient nitrogen photofixation, J. Mater. Chem. A 6 (2018) 4102–4110, https://doi.org/10.1039/C7TA09350K.
[40] Z. Meng, Y. Liu, G. Yang, Y. Cao, H. Wang, F. Peng, P. Liu, H. Yu, Electron-rich ruthenium on nitrogen-doped carbons promoting levulinic acid hydrogenation to γ-valerolactone: effect of metal-support interaction, ACS Sustain. Chem. Eng. 7 (2019) 16501–16510, https://doi.org/10.1021/acssuschemeng.9b03742.
[41] N. Karanwal, D. Verma, P. Butolia, S.M. Kim, J. Kim, One-pot direct conversion of levulinic acid into high-yield valeric acid over a highly stable bimetallic Nb-Cu/Zr-doped porous silica catalyst, Green Chem. 22 (2020) 766–787, https://doi.org/10.1039/c9gc03516h.
[42] D. Verma, R. Insyani, H.S. Cahyadi, J. Park, S.M. Kim, J.M. Cho, J.W. Bae, J. Kim, Ga-doped Cu/H-nanozeolite-Y catalyst for selective hydrogenation and hydrodeoxygenation of lignin-derived chemicals, Green Chem. 20 (2018) 3253–3270, https://doi.org/10.1039/c8gc00629f.
[43] Q. Liu, B. Qiao, F. Liu, L. Zhang, Y. Su, A. Wang, T. Zhang, Catalytic production of 1,4-pentanediol from furfural in a fixed-bed system under mild conditions, Green Chem. 22 (2020) 3532–3538, https://doi.org/10.1039/d0gc00233j.
[44] Y. Liu, G. Ding, G. Zhao, H. She, Y. Zhu, Y. Yang, Conversion of glucose to levulinic acid and upgradation to γ-valerolactone on Ru/TiO2catalysts, New J. Chem. 45 (2021) 14406–14413, https://doi.org/10.1039/d1nj01990b.
[45] Z. Tang, P. Liu, H. Cao, S. Bals, H.J. Heeres, P.P. Pescarmona, Pt/ZrO2 prepared by atomic trapping: an efficient catalyst for the conversion of glycerol to lactic acid with concomitant transfer hydrogenation of cyclohexene, ACS Catal. 9 (2019) 9953–9963, https://doi.org/10.1021/acscatal.9b02139.
[46] P.P. Upare, J.M. Lee, D.W. Hwang, S.B. Halligudi, Y.K. Hwang, J.S. Chang, Selective hydrogenation of levulinic acid to γ-valerolactone over carbon-supported noble metal catalysts, J. Ind. Eng. Chem. 17 (2011) 287–292, https://doi.org/10.1016/j.jiec.2011.02.025.
[47] J. An, G. Sun, H. Xia, Aerobic oxidation of 5-hydroxymethylfurfural to high-yield 5-Hydroxymethyl-2-furancarboxylic acid by poly(vinylpyrrolidone)-capped Ag nanoparticle catalysts, ACS Sustain. Chem. Eng. 7 (2019) 6696–6706, https://doi.org/10.1021/acssuschemeng.8b05916.
[48] S. Wei, A. Li, J.C. Liu, Z. Li, W. Chen, Y. Gong, Q. Zhang, W.C. Cheong, Y. Wang, L. Zheng, H. Xiao, C. Chen, D. Wang, Q. Peng, L. Gu, X. Han, J. Li, Y. Li, Direct observation of noble metal nanoparticles transforming to thermally stable single atoms, Nat. Nanotechnol. 13 (2018) 856–861, https://doi.org/10.1038/s41565-018-0197-9.
[49] Y. Zhang, T.L. Eberhardt, B. Cai, M. Wu, X. Xu, J. Feng, H. Pan, Organosolv fractionation of a lignocellulosic biomass feedstock using a pilot scale microwave-heating reactor, Ind. Crops Prod. 180 (2022), 114700, https://doi.org/10.1016/j.indcrop.2022.114700.
[50] X. Chang, A.F. Liu, B. Cai, J.Y. Luo, H. Pan, Y.B. Huang, Catalytic transfer hydrogenation of furfural to 2-methylfuran and 2-methyltetrahydrofuran over bimetallic copper–palladium catalysts, ChemSusChem 9 (2016) 3330–3337, https://doi.org/10.1002/cssc.201601122.
[51] Z. Yang, Y.-B. Huang, Q.-X. Guo, Y. Fu, RANEY® Ni catalyzed transfer hydrogenation of levulinate esters to γ-valerolactone at room temperature, Chem. Commun. 49 (2013) 5328, https://doi.org/10.1039/c3cc40980e.
[52] Z. Tong, X. Li, J. Dong, R. Gao, Q. Deng, J. Wang, Z. Zeng, J.J. Zou, S. Deng, Adsorption configuration-determined selective hydrogenative ring opening and ring rearrangement of furfural over metal phosphate, ACS Catal. 11 (2021), https://doi.org/10.1021/acscatal.0c05497.